Application of BPH zeolite for the transesterification of glycerol to glycerol carbonate: effect of morphology, cation type and reaction condition

Siriporn Kosawatthanakun, Edwin Clatworthy, Sajjad Ghojavand, Narongrit Sosa, Jatuporn Wittayakun, Svetlana Mintova

Application of BPH zeolite for the transesterification of glycerol to glycerol carbonate: effect of morphology, cation type and reaction condition

Siriporn Kosawatthanakun,[a] *Edwin B. Clatworthy,*[*b] *Sajjad Ghojavand,* [b] *Narongrit Sosa,*[ac] *Jatuporn Wittayakun,*[*a] *and Svetlana Mintova,*[b]

[a] School of Chemistry, Institute of Science, Suranaree University of Technology, Nakhon Ratchasima 30000, Thailand

[b] Normandie Université, ENSICAEN, UNICAEN, CNRS, Laboratoire Catalyse et Spectrochimie (LCS), 14050 Caen, France

[c] Nuclear Technology Research and Development Center, Thailand Institute of Nuclear Technology (Public Organization), Nakhon Nayok 26120, Thailand

KEYWORDS: nanozeolite, BPH zeolite, transesterification, glycerol, glycerol carbonate

ABSTRACT: The valorization of glycerol (Gly) to high-value chemicals is the key to unlocking economic and sustainable biodiesel production. Transesterification of Gly with dimethyl carbonate (DMC) to glycerol carbonate (GC) requires a catalyst with high basicity and uniform pore size for high product selectivity. BPH-type zeolite (Linde Q) nanosheets are promising catalysts for overcoming diffusion transport limitations inside the pore network and inhibiting the formation of glycidol as a side product. As-prepared BPH nanosheets (nano-sized CsBPH_AP, 192 nm size) and micron-sized BPH (micron-sized KBPH_AP, 600 nm size) were prepared by hydrothermal treatment with different Si/Al ratios. With a morphological-dependent reaction, nano-sized CsBPH_AP demonstrates superior performance in the transesterification of Gly to GC than micron-sized KBPH_AP. Ion-exchange of the nano-sized CsBPH_AP and micron-sized BPH_AP, with potassium and cesium precursors respectively, to afford nano-sized K-CsBPH_IE and micron-sized Cs-KBPH_IE resulted in similar thermal properties but different basicity and catalytic activity compared to the parent samples; higher basicity resulted in better catalytic performance. The nano-sized CsBPH_AP with a catalyst loading of 6 wt% shows good catalytic performance over four runs under optimized reaction conditions at 120 ºC for 3 h and Gly:DMC molar ratio of 1:5. This study reveals the crucial effect of catalyst morphology and size on the conversion of Gly to GC.

1. INTRODUCTION

Biodiesel has emerged as an attractive alternative to petroleum-derived fuels because of its production from renewable feedstocks such as animal and plant fats, and its potential to offset anthropogenic CO_2 emissions from non-renewable fossil fuels.[1] However, while the transesterification of glyceride and methanol produces three moles of biodiesel (fatty acid methyl esters), it also produces one mole of glycerol (Gly).[2] As a result of increased biodiesel production there have significant efforts to valorize Gly into high value-added chemicals such as acrolein by dehydration,[3] glycerol carbonate (GC) by transesterification,[4] and 1,3-propanediol by dehydroxylation.[5]

In particular, GC has received increasing attention due to its versatility as a platform molecule; it can be produced by the transesterification of Gly with dimethyl carbonate (DMC). Since DMC can serve as both a methylating agent and a solvent the reaction can be performed with or without a solvent. The reaction has been investigated in heterogeneous catalysis settings employing zeolites,[6-8] micro-mesoporous silicas,[3, 4] silicates,[9] titanosilicate,[10] and hydrotalcites.[11] Although these catalysts demonstrate high performance they suffer from limitations including the molecular diffusion of the reactants and products, and reduced accessibility of basic sites.[4] To address these issues, modification of the catalyst properties such as the zeolite pore diameter, particle size, and shape offers potential solutions.

Both zeolite-based and mesoporous catalysts have been investigated for GC production. Micron-sized chabazite (Si/Al = 2.4) in potassium form (K-CHA) consisting of aggregated quadratic prism-like crystals hydrothermally synthesized from coal fly ash gave a high yield of GC (96%) in solvent-free conditions without the leaching of metallic species (K, Ca, Ti, and Fe).[7] However, glycidol side product was formed due to the strong basicity of the catalyst.[7]

Although the pore size of chabazite (8-ring, 0.38 × 0.38 nm) is smaller than the sizes of the reactants and product (the geometric dimensions of Gly: 0.47 × 0.52 nm, DMC: 0.37 × 0.45 nm, GC: 0.33 × 0.65 nm),[8] the presence of mesopores could facilitate access to the active sites. The performance of Na-containing zeolites with different pore networks **(Scheme 1)** including 3A (8-ring, 0.31 × 0.35 nm), 4A (10-ring, 0.41 × 0.41 nm), NaZSM-5 (10-ring, 0.51 × 0.55 and 0.53 × 0.56 nm), NaBEA (12-ring, 0.66 × 0.67 and 0.56 × 0.56 nm), and NaY (12-ring, 0.74 × 0.74 nm) have also been investigated for catalyzing the production of GC from Gly and DMC. Those zeolites were micron-sized and the reaction was performed in methanol under reflux.[8] Both NaBEA and NaY were the only Na-containing zeolites reported to demonstrate the conversion of Gly to GC with 100% selectivity, of which NaY exhibited the best performance. This suggests that zeolites with large pores are preferable for the selective transesterification of Gly due to the geometric dimensions of Gly, DMC and GC.[8]

In addition to the size of the zeolite pores, the shape and size of the zeolite particles have been reported as significant factors in the conversion of Gly. By tuning the length of the crystal *b*-axis (60–70 nm), microporous H-ZSM-5 (Si/Al = 25–125) was utilized for Gly dehydration to acrolein.[3] Because of the shortened *b*-axis by an order of magnitude and thus the more rapid diffusion of molecules within the pore network, the catalyst exhibited a higher Gly conversion compared to a commercial ZSM-5 with a *b*-axis length of 1.5–1.7 μm. In addition to zeolites, mesoporous silicas containing layered double hydroxides (LDH) with three different morphologies (rice-shaped, short rods, and long rods), were proposed as nanosized composites for the transesterification of Gly with DMC in dimethyl formamide (DMF).[4] The rice-shaped catalyst with relatively shorter mesoporous channels improved the internal diffusion path lengths of both the reactants and products. Moreover, the relatively higher specific surface area of the

rice-shaped nanosized composite allowed for a high density of surface basic sites, resulting in superior catalytic activity compared to the rod-shaped catalysts. This demonstrates how facilitating rapid and facile access to the basic sites by controlling the catalyst morphology is critical to achieving both high Gly conversion and GC selectivity. Furthermore, catalyst nano-structuring to achieve improved access to active sites and enhanced molecular diffusion can provide additional strategies for tailoring the catalyst behavior for Gly conversion reactions. Sulfonated porous carbons prepared from silica/resin nanocomposites exhibited greater catalytic performance compared to conventional solid acid catalysts for Gly acetylization. Despite having a lower acid site concentration the hollow sphere morphology of the sulfonated porous carbons afforded superior mass transfer properties compared to the conventional catalysts.[12] Concerning mesoporosity, the introduction of hierarchical structure to ZSM-5 zeolite catalysts and the effects on the catalytic performance on the dehydration of Gly to acrolein have shown that the type of mesoporosity formed significantly influences the catalytic performance.[13] The sample with open and interconnected mesopores demonstrated better catalytic performance compared to the sample with closed and small mesopores, attributed to differences in their mass transfer properties and in-pore condensation of the reactant.

To achieve the targeted conversion of Gly to GC using environment-friendly catalysis, intrinsically basic nanosized zeolites with specific morphology present as attractive candidates as catalysts. At present, there is no report on the utilization of BPH zeolite nanosheets (Linde Q) for Gly conversion. The low-silica nanosheets possesses an appropriately-sized 12-membered ring (12MR) pore aperture along the *c*-axis of 0.63 × 0.63 nm, which is greater than the geometric diameters of Gly, DMC and GC (**Scheme 1**).[14] The 12MR channel is perpendicularly intersected by three eight-membered rings channels.[15] Initially, conventional micron-sized BPH zeolite,

prepared from a K^+-containing alkaline aluminosilicate precursor mixture, was not considered for catalytic applications due to its low thermal stability as a result of its high framework aluminum content (Si/Al = 1).[15, 16] However, by employing organic templates during the synthesis procedure followed by post-synthetic treatments, higher silica-containing (Si/Al ratio up to 10) and acidic variants of BPH zeolite (UZM-4) were produced.[17-19] The post-synthetically treated zeolites were shown to be active for heptane cracking between 450 and 550 °C. In this work, the BPH nanosheets are prepared without organic structure-directing agents under mild (60 ºC) conditions with a relatively short synthesis time, and do not require post-synthetic template removal by calcination.[20] Importantly, as a consequence of their morphology the BPH nanosheets can offer a shorter molecular diffusion path length than the other zeolites described above.

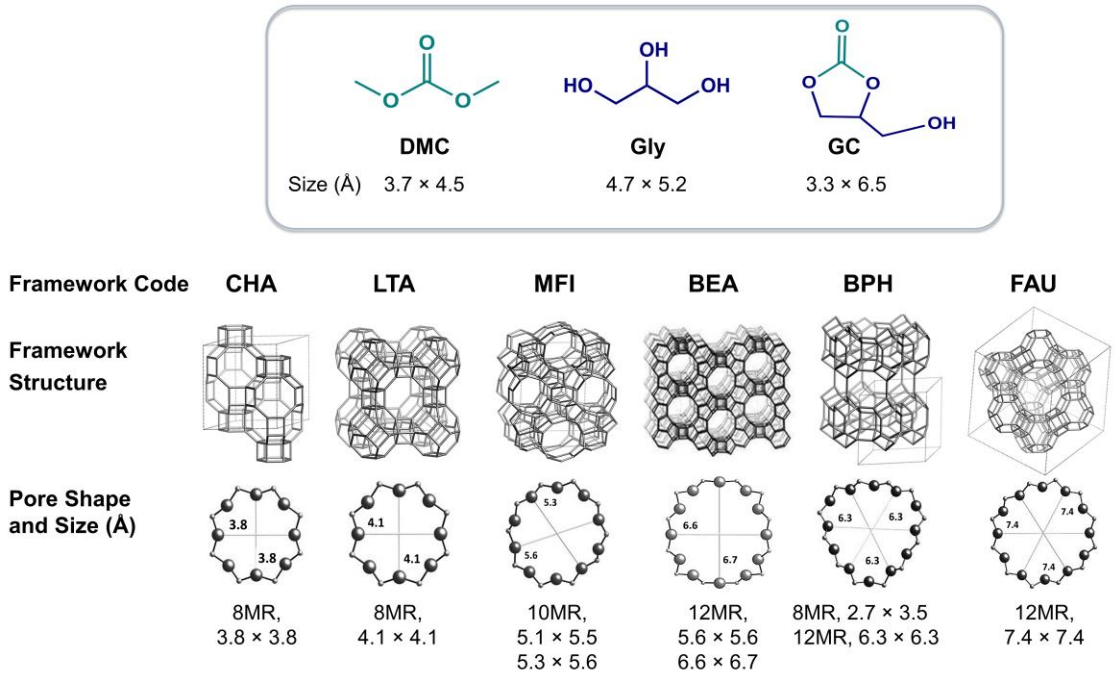

Scheme 1. Comparison of the sizes of DMC, Gly and GC, and the comparison of the zeolite frameworks, including pore shapes and sizes, studied previously and in this work (BPH) for the conversion of Gly to GC.

Herein, BPH zeolites with different morphologies (nanosheets and micron-sized plates) were studied in terms of the correlation of their morphologies and sizes with their catalytic performance. Their intrinsic basic properties were adjustable by ion-exchanging with alkali metal cations. Their catalytic activities were investigated in the transesterification of Gly with DMC without the use of an additional solvent. The reaction factors affecting the catalytic performance including the catalyst morphology, reactant mole ratios, catalyst loading, reaction temperature and time, and reusability were explored.

2. EXPERIMENTAL SECTION

2.1. Chemicals and Materials

All reagents and solvents were used as received without any further purification: aluminum hydroxide ($Al(OH)_3$, extra pure, Acros Organics), LUDOX® AS-40 colloidal silica (SiO_2, Aldrich, 40 wt% suspension), cesium chloride (CsCl, 99.9%, Alfa Aesar), dimethyl carbonate (99%, Alfa Aesar), glycerol ($C_3H_8O_3$, 99.5%, Alfa Aesar) potassium silicate (K_2SiO_3, anhydrous ~48 Mesh, SiO_2:K_2O 2.5:1 wt%, Alfa Aesar), ethanol (C_2H_5OH, 99.9%, Carlo Erba), methanol (CH_3OH, 99%, Carlo Erba), cesium nitrate ($CsNO_3$, 99%, Sigma Aldrich), glycerol carbonate ($C_4H_6O_4$, 90%, Sigma Aldrich), glycidol ($C_3H_6O_2$, ≥95.0%, Sigma Aldrich), sulfuric acid (H_2SO_4, 98%), potassium hydroxide (KOH, 90%, Sigma Aldrich), potassium nitrate (KNO_3, 99%, Sigma Aldrich), sodium aluminate ($NaAlO_2$, 50–56% Al_2O_3, 40–45% Na_2O, Sigma-Aldrich), and sodium hydroxide (NaOH, 99%, VWR Chemicals). An aqueous solution of cesium hydroxide (CsOH, 50 wt% Cs) was prepared by dissolving cesium hydroxide hydrate ($CsOH \cdot xH_2O$ (15–20% H_2O), 99.9%, Alfa Aesar) in double-distilled water. All water used was double distilled using Aquatron water still A4000D.

2.2. Synthesis of nano-sized BPH zeolite

Nano-sized BPH zeolite was synthesized according to Clatworthy *et al.*[20] with the molar oxide composition of 0.3 Cs_2O: 1.25 K_2O: 8.07 Na_2O: 10 SiO_2: 0.8 Al_2O_3: 120 H_2O. The alkali aluminate mixture was prepared by dissolving 0.518 g of sodium aluminate and 3.78 g of double distilled water, followed by mixing 1.78 g of sodium hydroxide, 0.495 g of potassium hydroxide, and 0.506 g of cesium hydroxide solution (50 wt% Cs) in a sealed 60 mL polypropylene bottle. The aluminate solution was rapidly stirred for 2 h at room temperature until a clear solution was obtained. After that, 4.77 g of colloidal SiO_2 was added dropwise with vigorous stirring to the clear aluminate solution, resulting in a turbid mixture. The mixture was vigorously stirred for 24 h followed by hydrothermal treatment at 60 ºC for 16 h. The zeolite product was centrifuged at 20,000 rpm for 20 min, washed with double distilled water until the pH of the supernatant was ~7–8, and dried in an oven at 60 ºC overnight. The as-prepared BPH zeolite nanosheets are denoted as nano-sized CsBPH_AP.

2.3. Synthesis of micron-sized BPH (Linde Q)

The molar oxide composition for the synthesis of the micron-sized BPH was: 16 K_2O: 4 SiO_2: 1 Al_2O_3: 192 H_2O.[20] Potassium silicate solution was prepared by adding 6.47 g of potassium silicate to 23.92 g of double-distilled water. Then, the mixture was stirred overnight, followed by heating at 60 ºC for 30 min. The potassium aluminate solution was prepared by dissolving 3.00 g of aluminum hydroxide and 35.92 g of potassium hydroxide in 42.60 g of double distilled water, followed by heating at 90 ºC for 30 min. After allowing each solution to cool to room temperature, the potassium aluminate solution was slowly added to the potassium silicate solution with rapid stirring to form a cloudy gel. The gel was treated hydrothermally at 50 ºC for 162 h. The product was collected and washed by centrifugation at 20,000 rpm for 20 min with double distilled water until the pH of the supernatant was ~7–8. The product was dried

in an oven at 60 ºC overnight. The as-prepared micron-sized BPH zeolite is denoted micron-sized KBPH_AP.

2.4. Ion-exchange of BPH zeolite

Nano-sized CsBPH_AP (5 wt% solid) was ion-exchanged with 25 g of potassium solution (pH 9.8) containing 5 mM mixed solution of KNO_3 and KOH (10:1 w/w). For the micron-sized BPH_AP (5 wt% solid), cesium solution ($CsNO_3$:CsOH = 10:1 w/w) was used. Each mixture was stirred at room temperature for 1 h, washed with double distilled water and centrifuged at 20,000 rpm for 20 min until the pH of the supernatant was ~7–8. This procedure was repeated twice and the samples dried at 60 °C overnight. The ion-exchanged nano-sized CsBPH_AP and micron-sized BPH_AP zeolite are named nano-sized K-CsBPH_IE and micron-sized Cs-KBPH_IE, respectively.

2.5. Catalyst characterization

The crystalline structure of the samples was determined by powder X-ray diffraction (XRD) with a PANalytical X'Pert PRO-MPD diffractometer with Cu Kα radiation (λ = 1.5418 Å). All patterns were collected across a 2θ range of 4–50º with a step size of 0.0167º and time per step of 950 s. The particle morphology of the zeolite samples was analyzed by field emission scanning electron microscopy (FE-SEM) using a Zeiss AURIGA FE-SEM/FIB/EDX with an upper electron detector operating at an accelerated voltage of 3 kV with a working distance of 7.1 mm. Each sample was placed on carbon tape adhered to a copper stub. The sample was coated with gold using an operating current at 10 mA under an argon atmosphere for 5 min. The particle size distribution was processed by ImageJ software version 1.49.

Zeolite samples were analyzed by Fourier-transform infrared spectroscopy (FTIR) with a microscope on a Bruker Tensor27-Hyperion using ATR mode with a resolution of 4 cm^{-1} and 64

scans, samples were dried at 90 °C overnight before analysis. Thermogravimetric analysis was performed by a Setsys SETARAM analyzer. The samples (5–10 mg) were placed in an alumina crucible and heated from 30–800 ºC with a heating rate of 5 ºC·min^{-1} under a dry air flow of 40 mL·min^{-1}. The chemical composition of the samples was determined by inductively coupled plasma mass spectrometry (ICP-MS) using a 7900 ICP-MS from Agilent Technologies.

The basicity of the catalysts was investigated by temperature-programmed desorption of carbon dioxide (CO_2-TPD) using a BELCAT-B chemisorption analyzer. A 50 mg sample was packed into a tubular glass reactor and pretreated at 150 ºC under helium gas flow at 30 mL·min^{-1} for 180 min to eliminate physisorbed species. Then, the sample was cooled down to 50 ºC and a gas mixture of 10% CO_2/He was adsorbed onto the catalyst surface for 90 min. The sample was purged with He and held for 30 min to remove non-adsorbed CO_2. The desorbed CO_2 was quantified by the TPD process in the temperature range from 50 to 150 ºC with a ramp of 5 ºC·min^{-1} and held at 150 ºC for 120 min with a flow rate of 30 mL·min^{-1}. The basicity was obtained by integration of the peak area. In addition, the basic strength was analyzed by Hammett indicator.[21, 22] The indicators were bromothymol Blue (H_= 7.2) and phenolphthalein (H_= 9.8). Approximately 300 mg of sample was mixed with 10 mL of methanol containing 1 mL of the Hammett indicator and stirred for 2 hours to reach equilibrium. The color change of the solution was observed by the naked eye. The basic strengths are described as stronger than the weakest indicator that provides a color change, but weaker than the strongest indicator that makes no color change.

N_2 sorption analysis of samples was determined using Micromeritics 3Flex physisorption instrument at -196 °C. The fresh and reused samples were degassed at 300 ºC under vacuum for 8 h, nano-sized K-CsBPH_IE was degassed at 350 ºC under vacuum for 8 h, and micron-sized

BPH zeolite were degassed at 120 ºC under vacuum for 24 h. The data were processed with 3Flex version 5.02 software.

^{27}Al MAS NMR spectra were recorded on a Bruker Advance III-HD 500 (11.7 T) spectrometer using 4 mm-OD zirconia rotors. ^{27}Al MAS NMR was done with a π/12 pulse (selective pulse), a spinning speed of 14 kHz and a recycle delay of 1 s. Prior to measurement, the samples were fully hydrated in a water vapor-saturated chamber at ambient temperature. $Al(NO_3)_3$ (1 M) was used as a chemical shift reference for ^{27}Al nuclei. All spectra were normalized.

2.6. Transesterification of glycerol with dimethyl carbonate

Transesterification of glycerol (Gly) and dimethyl carbonate (DMC) to yield glycerol carbonate (GC) was performed by adding 1.50 g (16.3 mmol) of glycerol, 4.40 g (48.8 mmol) of DMC, and 0.12 g of catalyst (8 wt% compared to the amount of glycerol used) in a heavy wall pressure vessel at atmospheric pressure. The catalyst screening was carried out at 120 ºC in a silicone oil bath for 3 h, stirring at 800 rpm. The best catalyst, under the aforementioned conditions, was studied to determine the optimum reaction conditions including reaction temperature, time, catalyst loading, Gly:DMC ratio, and catalyst recyclability. After the reaction the product mixture was separated from the catalysts by centrifugation. The separated catalyst was washed with ethanol and double distilled water, dried in an oven at 80 ºC overnight and used for the next run.

The products were determined by high-performance liquid chromatography (1260 Infinity II LC System, Agilent) equipped with an Aminex HPX-87H column and a refractive index detector. An aqueous H_2SO_4 solution (5 mM) was the mobile phase with a flow rate of 0.60 $mL \cdot min^{-1}$ and a column temperature of 55 ºC. When Gly is the limiting reactant, Gly

conversion, GC yield, and selectivity of GC are calculated using equations 1, 2 and 3, respectively.

$$\text{Glycerol conversion (\%)} = \frac{\text{Mole of glycerol added} - \text{mole of remaning glycerol}}{\text{Mole of glycerol added}} \times 100 \quad (1)$$

$$\text{GC yield (\%)} = \frac{\text{Mole of GC produced}}{\text{Mole of glycerol added}} \times 100 \quad (2)$$

$$\text{GC selectivity (\%)} = \frac{\text{GC yield}}{\text{Glycerol conversion}} \times 100 \quad (3)$$

3. RESULTS AND DISCUSSION

3.1. Characterization of the catalysts

XRD patterns of the nano- and micron-sized BPH zeolite samples are shown in **Fig. 1**. All samples possess the BPH framework topology. The diffraction patterns of the nano-sized CsBPH_AP have relatively less intensity and broader peaks than the micron-sized BPH due to the smaller crystalline domains[20]; this is further confirmed by SEM analysis (*vide infra*). In particular, the (001) reflection of the nanosheets at 2θ of ≈ 6.4º has a very low intensity due to the significantly reduced sheet thickness compared to the micron-sized BPH sample. The XRD patterns of the ion-exchanged samples are not significantly different from those of the parent samples. This indicates that the crystal structure and the morphology of the samples are preserved during the ion-exchange process.

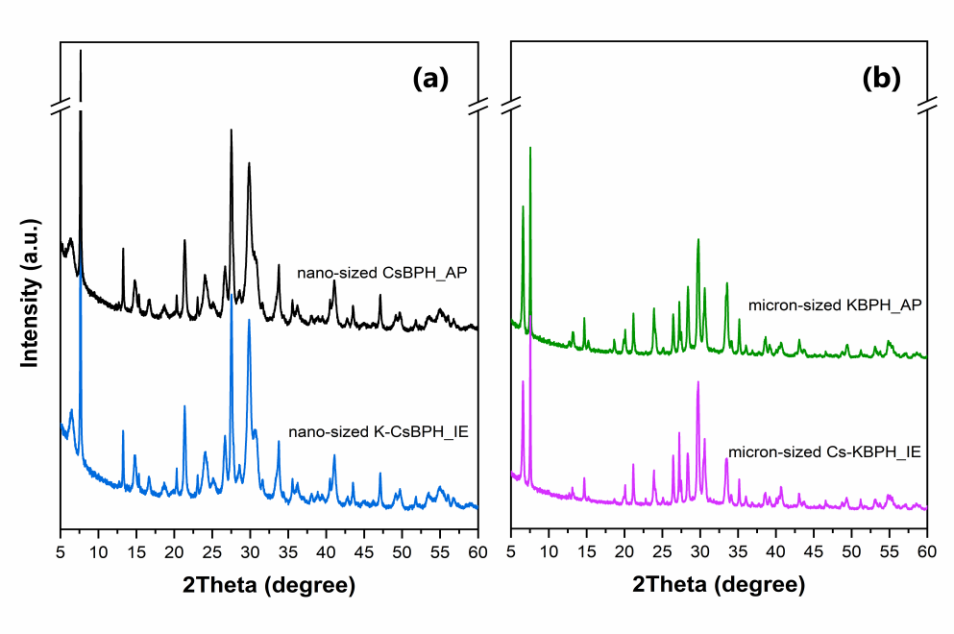

Fig. 1 XRD patterns of (a) nano-sized CsBPH_AP (black) and nano-sized K-CsBPH_IE (blue) and (b) micron-sized KBPH_AP (green) and micron-sized Cs-KBPH_IE (purple).

SEM images of the nano- and micron-sized BPH zeolite samples are presented in **Fig. 2**. The nano-sized CsBPH_AP sample is described by agglomerated nano-sized sheets with dimensions of 192±15 nm across and 20±3 nm thick. The morphology is similar to the nano-sized BPH zeolite reported by Clatworthy *et al.*[20] The micron-sized KBPH_AP is described by plate-like particles 541±40 nm across and 57±9 nm thick. The SEM analysis of the BPH zeolite samples demonstrates the different sizes of the zeolite particles which could play a role in determining their catalytic performance. A smaller particle size generally facilitates more rapid diffusion of the reactants and products through the zeolite pore network.

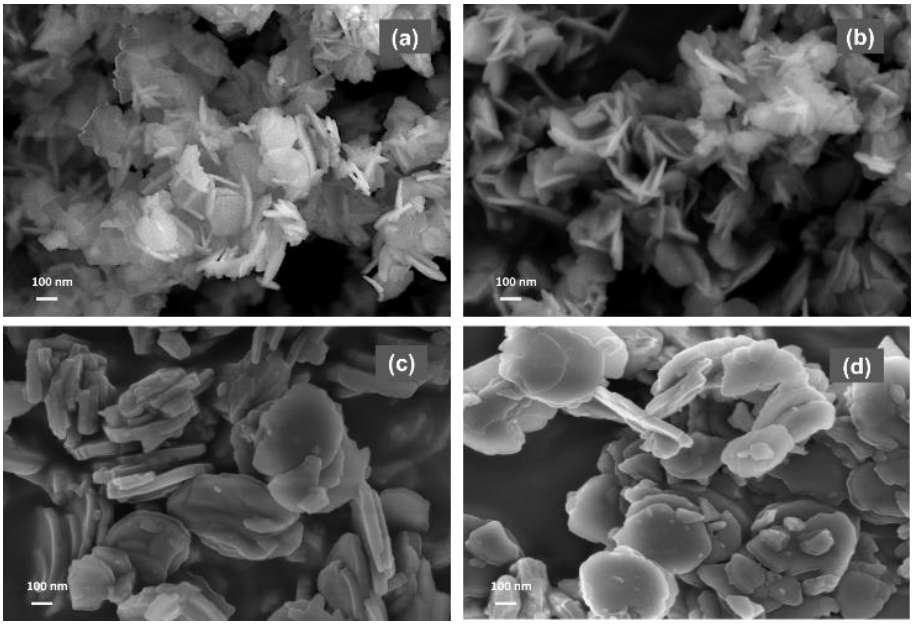

Fig. 2 SEM images of (a) nano-sized CsBPH_AP, (b) nano-sized K-CsBPH_IE, (c) micron-sized KBPH_AP, and (d) micron-sized Cs-KBPH_IE.

From the ICP analysis presented in **Table 1**, the sodium content from the nano-sized K-CsBPH_IE slightly decreased after ion exchange with potassium solution. Meanwhile, the cesium amount from micron-sized Cs-KBPH_IE increased after ion exchange with cesium solution. Although the BPH-type zeolite nanosheets were ion exchanged with a different alkali metal solutions, the original type of alkali metal cations (Na^+, K^+, Cs^+) were preserved, in part due to their strong ionic interaction with the zeolite structure.[23, 24] The nano-sized CsBPH_AP sample has a higher Si/Al molar ratio than the micron-sized KBPH_AP which is likely a reflection of the different Si and Al contents of the synthesis recipies. After the ion-exchange process the Si/Al ratio of the ion-exchanged zeolites was found to be unchanged compared to the parent samples.

Table 1. Elemental composition of BPH-type zeolite samples determined by ICP-MS, and basicity measured by CO_2-TPD.

Catalyst	Composition	Si/Al ratio (mol)	Basicity (mmol $CO_2 \cdot g^{-1}$)
micron-sized KBPH_AP	$(K_{14})Si_{14}Al_{14}O_{56}$	1.00	0.327
micron-sized Cs-KBPH_IE	$(CsK_{13})Si_{14}Al_{14}O_{56}$	1.00	0.350
nano-sized CsBPH_AP	$(Cs_{4.2}K_{2.3}Na_{5.5})Si_{16}Al_{12}O_{56}$	1.33	0.130
nano-sized K-CsBPH_IE	$(Cs_{4.2}K_{3.3}Na_{4.5})Si_{16}Al_{12}O_{56}$	1.33	0.105

The FTIR spectra of the as-prepared and ion-exchanged BPH zeolites are presented in **Fig. 3.** The nano-sized CsBPH_AP and micron-sized KBPH_AP have similar FTIR spectra but different peak positions due to their different Si/Al ratios.[25] The characteristic bands of BPH zeolite at 1150–950 cm^{-1} and 740–660 cm^{-1} are attributed to the asymmetric and symmetric stretching of the zeolite framework, respectively. The bands at 496, and 415–410 cm^{-1} are assigned to the bending mode of Si–O–T, where T is a framework Si or Al atom.[26] An intense band at 598–588 cm^{-1} is typically associated with double rings. Although BPH does not possess double rings, this band could be ascribed to the vibration of six rings in the *afs* and *bph* composite building units.[27] Moreover, the bands from OH groups or water are observed at 1649 and 3400 cm^{-1}. The FTIR spectra of the nano-sized K-CsBPH_IE and micron-sized Cs-KBPH_IE are similar to their parent zeolites; no significant differences are observed.

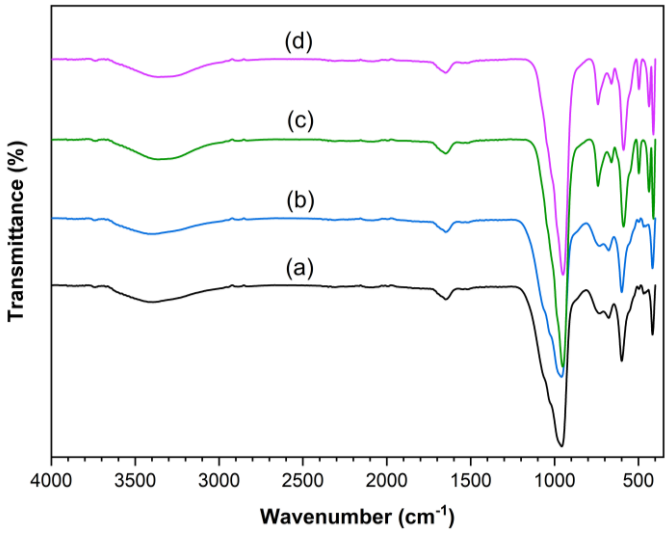

Fig. 3 FTIR spectra of (a) nano-sized CsBPH_AP, (b) nano-sized K-CsBPH_IE, (c) micron-sized KBPH_AP, and (d) micron-sized Cs-KBPH_IE.

The thermal properties of the BPH zeolite samples determined by thermogravimetric analysis in air are presented in **Fig. 4** and are similar to those previously reported under vacuum.[20] The nano-sized CsBPH_AP sample displays significant mass loss below 130 °C due to the removal of surface and physisorbed water; further mass loss to ~300 °C is due to the removal of cation-coordinated water. In comparison, the micron-sized KBPH_AP sample exhibits a lower degree of mass loss below 110 ºC followed by a second event at 220 ºC. The difference in the mass loss behavior is related to the difference in the zeolite external surface areas, diffusion path length of water through the zeolites, and extra-framework cation compositions. At 350 ºC both samples show complete removal of the physisorbed and chemisorbed water. Both the potassium-exchanged nano-sized K-CsBPH_IE and cesium-exchanged micron-sized Cs-KBPH_IE exhibit a similar mass loss at 350 °C compared to their parent samples (16.3 *vs* 15.6% and 15.1 *vs* 15.7% respectively) due to their similar chemical compositions.

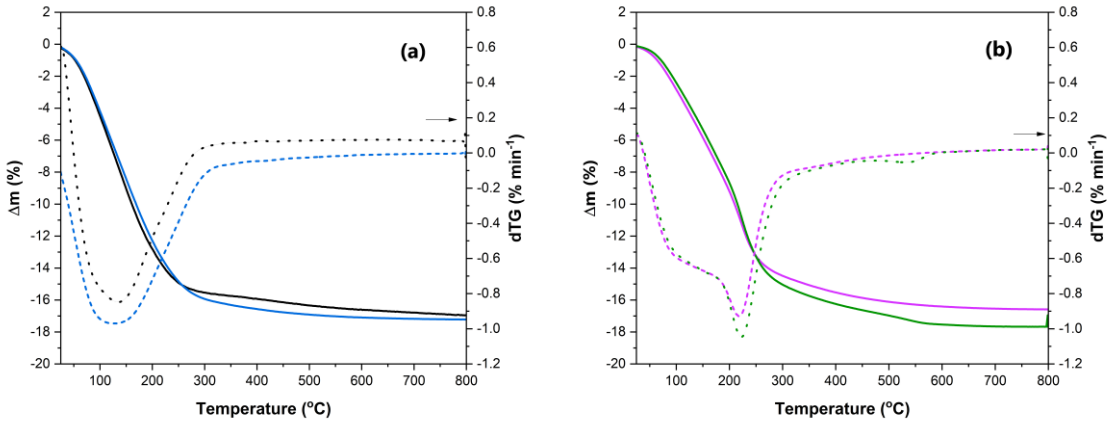

Fig. 4 TG and dTG profiles of the BPH zeolite samples (a) nano-sized CsBPH_AP (black) and nano-sized K-CsBPH_IE (blue) and (b) micron-sized KBPH_AP (green) and micron-sized Cs-KBPH_IE (purple).

The CO_2-TPD profiles of the as-prepared and ion-exchanged BPH zeolites are shown in **Fig. 5** and the basicities are listed in **Table 1**. Micron-sized KBPH_AP and nano-sized CsBPH_AP show a desorption peak at 93 ºC and 94 ºC, respectively, indicating no difference in interaction with the probe molecule CO_2. However, micron-sized KBPH_AP shows stronger intrinsic basicity because of a lower Si/Al ratio.[28-30] After ion exchange, the CO_2-TPD profiles of the micron-sized Cs-KBPH_IE and nano-sized K-CsBPH_IE exhibit slight changes compared to their parent samples. With a higher Cs content, micron-sized Cs-KBPH_IE provides stronger basicity than micron-sized KBPH_AP. The results are consistent with the case of CO_2 adsorption on zeolite Y at low pressure, whereby the basicity of the zeolite framework oxygens decreases with decreasing size of the extra-framework cation, *i.e.* from Cs^+ to Li^+. The simultaneous interaction of CO_2 with Cs^+ and neighboring framework oxygen atoms on CsY stabilizes CO_2 adsorption more than that on KY.[31, 32] However, the nano-sized K-CsBPH_IE exhibits a slightly lower basicity compared to the parent sample despite the exchange of approximately one Na^+ for

K^+. This is likely a consequence of the coordination environment of the extra-framework cation and adsorbed CO_2; the structure determination of this material is ongoing.

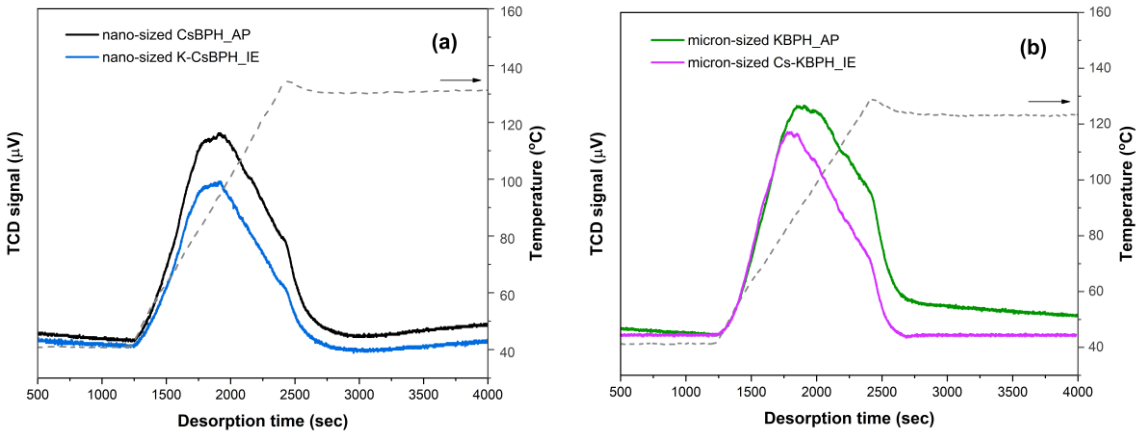

Fig. 5 CO_2-TPD profiles of (a) nano-sized CsBPH_AP (black) and nano-sized K-CsBPH_IE (blue) and (b) micron-sized KBPH_AP (green) and micron-sized Cs-KBPH_IE (purple).

The basicity was also analyzed by Hammett indicator. The basic strength (H_) of all samples was in the same range, 7.2 < H_ < 9.3. From the color of the indicator in **Fig. S1**, the basic strength order was in the following order: micron-sized KBPH_AP ≈ micron-sized Cs-KBPH_IE > nano-sized CsBPH_AP ≈ nano-sized K-CsBPH_IE.

3.2. Catalytic activity for the transesterification of glycerol with DMC

3.2.1. Catalyst screening

A comparison of the BPH zeolite samples with different particle sizes (micron *vs* nano) and cation contents on the performance in the transesterification of Gly with DMC is presented in **Fig. 6**. A blank reaction without catalyst affords a poor conversion of Gly and a low yield of the GC product. This result is consistent with the literature that the reaction performed without catalyst at 70 ºC in methanol under reflux did not show Gly conversion and selectivity towards GC; in another work a small GC yield (≈1%) was detected at 100 ºC.[8, 11] The higher reaction

temperature used in this work is responsible for the observed low Gly conversion and GC yield for the catalyst-free run.[33]

Considering the difference in the particle size of the BPH zeolite samples only, nano-sized CsBPH_AP and nano-sized K-CsBPH_IE demonstrate better transesterification performance for the conversion of Gly and yield of GC than micron-sized KBPH_AP and micron-sized Cs-KBPH_IE. The better performance could be attributed to the shorter diffusion paths of the reagents and larger surface areas, which is the advantage of nano- over micron-sized zeolites.[34] To the best of our knowledge, this is the first report comparing nano- and micron-sized zeolites for the transesterification of Gly to GC. The effect of the catalyst particle shape and size was reported by She *et al.*[4] The rice-shaped LDH/SBA-15 nanocomposite showed higher activity due to the greater specific surface area and reduced diffusion path length of the reactants and products compared to the other morphologies investigated.

The effect of basicity on the performance of the BPH zeolite catalysts by varying the extra-framework cation content is compared in **Fig. 6**. After ion exchange of the nano-sized CsBPH_AP with K^+, the obtained nano-sized K-CsBPH_IE demonstrated a lower catalytic activity than the nano-sized CsBPH_AP. In contrast by introducing Cs^+ to the micron-sized KBPH_AP, micron-sized Cs-KBPH_IE showed a higher activity than the parent KBPH. The catalytic performances are consistent with the basicity from CO_2-TPD (Table 1 and Figure 5). This finding is in good agreement with the report by Al-Ani *et al.*[28] on the basicity of ion-exchanged FAU and performance in transesterification of rapeseed oil with methanol.

From these results, not only is the morphology of the BPH nanosheets is crucial, but the basicity is also key to optimizing the transesterification of Gly with DMC. From the results, the nano-sized CsBPH_AP catalyst was subject to further study.

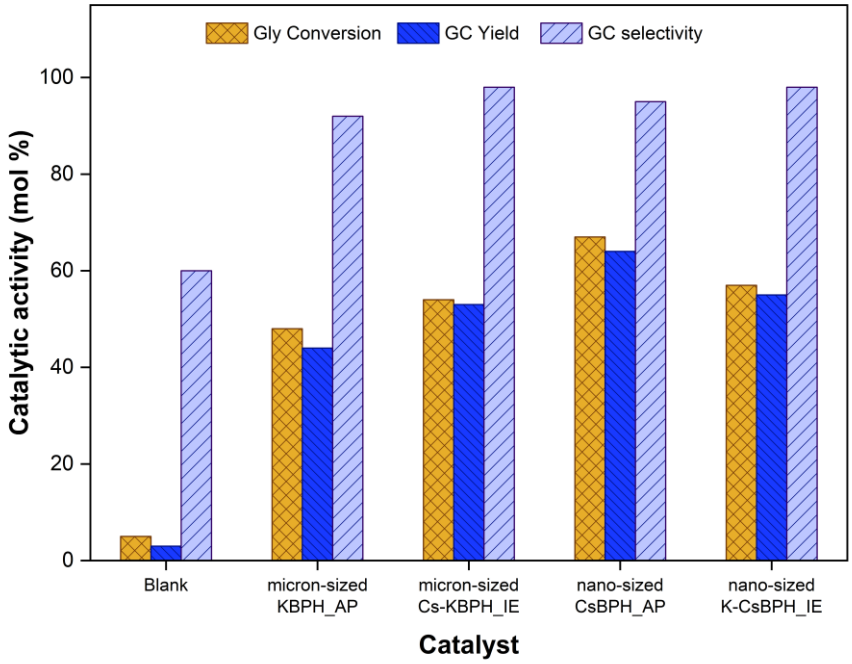

Fig. 6 Comparison of the as-prepared and ion-exchanged micron-sized and nano-sized BPH zeolite samples for the transesterification of Gly with DMC. Reaction conditions: 120 ºC, 3 h, Gly:DMC molar ratio of 1:3, catalyst loading of 8 wt%.

3.2.2. Effect of different reaction parameters on the transesterification

The effect of the reaction temperature across the range of 90–135 ºC on the transesterification of Gly with DMC using the nano-sized CsBPH_AP catalyst is shown in **Fig. 7a**. The Gly conversion and GC yield increase with the temperature, indicating that the reaction is endothermic. A similar effect was observed from the reaction catalyzed by transition-metal doped hydrotalcite[11] and K-CHA.[7] The viscosity of reactants is reduced at a higher temperature, resulting in better miscibility of Gly and DMC. Although the Gly conversion and GC yield further increase at the reaction temperature of 135 ºC, the selectivity towards GC decreases due to the formation of side products. The results indicate that a reaction temperature above 120 ºC is

not suitable. Accordingly, the optimal temperature for the transesterification of Gly and DMC catalyzed by nano-sized CsBPH_AP is 120 ºC.

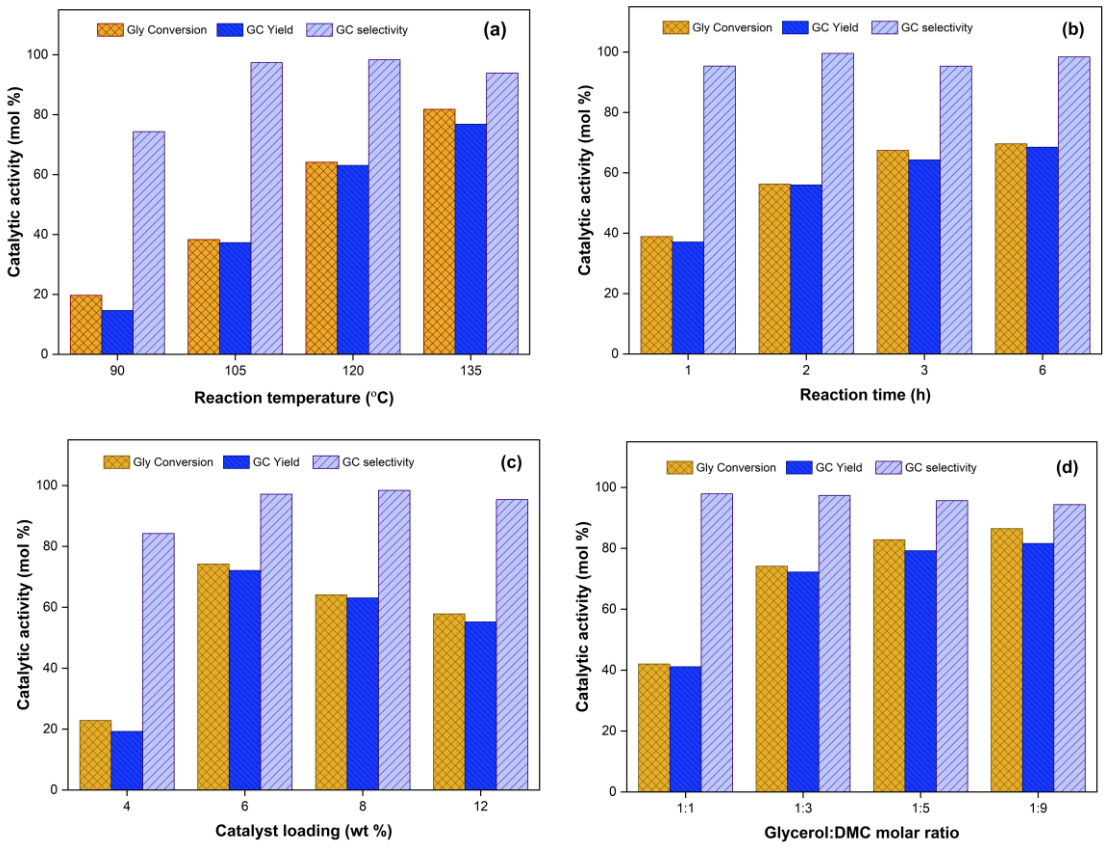

Fig. 7 Effects of different reaction parameters on the transesterification of Gly with DMC using the nano-sized CsBPH_AP catalyst: (a) effect of temperature at Gly:DMC molar ratio of 1:3, 8 wt% catalyst, 3 h; (b) effect of time at Gly:DMC molar ratio of 1:3, 8 wt% catalyst, 120 ºC; (c) effect of catalyst loading at Gly:DMC molar ratio of 1:3, 120 ºC, 3 h; (d) effect of Gly:DMC molar ratio at 6 wt% catalyst, 120 ºC, 3 h.

The effect of the reaction time from 1 to 6 h on the transesterification of Gly with DMC over the nano-sized CsBPH_AP catalyst is presented in **Fig. 7b**. The Gly conversion and the GC yield increase with the reaction time. The performance at 6 h was slightly higher than that at 3 h, indicating the equilibrium was approached. In comparison with the literature, the time to reach

the equilibrium varied with the reaction conditions such as temperature, type of reactor, mole ratio of reactants, and type and loading of catalyst. For example, to reach equilibrium over NaY under reflux at 70 ºC required 4 h,[8] but 1.5 h over KCHA at 75 ºC.[7] The longer reaction time might lead to a decrease in the GC selectivity due to the formation of side products.[7] Considering the significant increase of the reaction activity with time, the duration of 3 h is suitable for further evaluation.

The comparison of catalyst loading across the range of 4–12 wt% on the transesterification of Gly with DMC using the nano-sized CsBPH_AP catalyst is shown in **Fig. 7c**. Both Gly conversion and GC yield increase dramatically with the loading from 4 to 6 wt%. This could be from the increase in the concentration of active basic sites that initiate Gly transesterification by abstracting its proton from the first hydroxyl group.[7] The catalyst loading beyond 6 wt% results in the decline of activity in a linear manner. This is possibly due to the increased viscosity of the mixture and the adsorption of the reactants and products on the catalyst surface. In addition, the change in catalyst loading from 4 to 12 wt% does not affect the selectivity of the GC product. From these results, the optimal catalyst loading is 6 wt%.

The comparison of the molar ratios of glycerol to DMC on the transesterification is presented in **Fig. 7d**. At the equivalent molar ratio, both Gly conversion and GC yield are below 50 mol% due to the increased viscosity and poor mass transfer of reactants in the reaction system. At a molar ratio of glycerol to DMC above 1:3, the reaction activity increases because the higher molar ratio could shift the reaction equilibrium towards the GC product.[7, 22, 35] Considering the reaction setup, the Gly:DMC molar ratio of 1:5 facilitates the magnetic stirring by decreasing the mixture viscosity. Finally, the molar ratio of 1:9 provides an excess amount of

DMC that does not affect the reaction activity. The Gly conversion and GC products are slightly increased.

The results from the catalytic testing demonstrate that the nano-sized CsBPH_AP, identified as the best catalyst in this work from the optimal reaction conditions, has potential as a catalyst for the transesterification of Gly among the catalysts already reported in the literature (Table S2).

3.2.3. Reusability of the catalyst

The reusability and leaching tests of the nano-sized CsBPH_AP catalyst for the transesterification of Gly with DMC with the optimal reaction conditions are shown in **Fig. 8a**. The nano-sized CsBPH-AP retains its initial catalytic performance in the first two runs followed by a decrease of the Gly conversion and GC yield by 14% and 13%, respectively. However, the GC selectivity remains constant across all four runs. The results show that the nano-sized CsBPH_AP catalyst is susceptible to activity loss during transesterification. The leaching test was performed to investigate the catalyst stability by separating the nano-sized BPH zeolite catalyst by hot filtration after 1 h of reaction while the filtrate was kept under the same reaction conditions without the catalyst for another 2 h. The analysis of the reaction mixture revealed no further glycerol conversion after the removal of the nano-sized BPH zeolite catalyst, demonstrating that leaching was not the cause of deactivation (**Fig. 8b**).

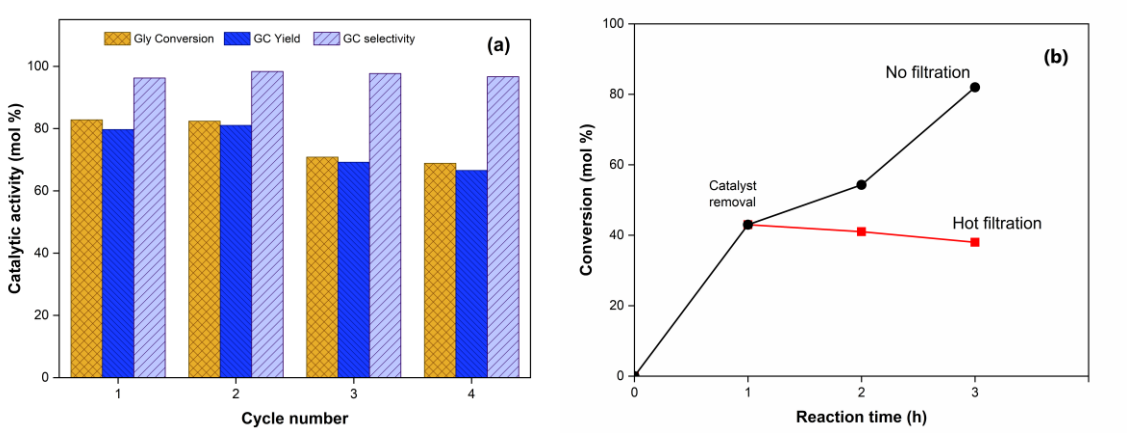

Fig. 8 (a) Reusability and (b) leaching tests of the nano-sized CsBPH_AP catalyst under the conditions: 120 ºC for 3 h; Gly:DMC molar ratio of 1:5; catalyst loading of 6 wt%.

The nano-sized CsBPH_AP catalyst was analyzed after the fourth run by XRD, FTIR, TGA, N_2 sorption, ^{27}Al MAS NMR and CO_2-TPD. The results from each technique were compared with that of the fresh catalyst in **Fig. 9**. The reused and fresh nano-sized CsBPH_AP show similar results from XRD, FTIR, TGA, and N_2 sorption (**Fig. 9a-d**, respectively). In addition, ICP-MS analysis of the nano-sized Cs-BPH_AP catalyst after the fourth reaction cycle revealed negligible differences in the composition between the fresh ($(Cs_{4.2}K_{2.3}Na_{5.5})Si_{16}Al_{12}O_{56}$) and used ($(Cs_{4.2}K_{2.3}Na_{5.7})Si_{15.7}Al_{12.2}O_{56}$) catalysts. This suggests that the structure of the nano-sized CsBPH_AP is stable under the catalytic test conditions, making it a good candidate for further development. However, the reused sample has a lower basicity according to the CO_2-TPD profiles and slightly lower intensity in ^{27}Al NMR spectra (**Fig. 9e-f**, respectively). The results suggest that the cause of deactivation could be dealumination. As a consequence, further investigation to understand the changes during the reaction is necessary to find ways to retain the catalyst performance over a greater number of runs.

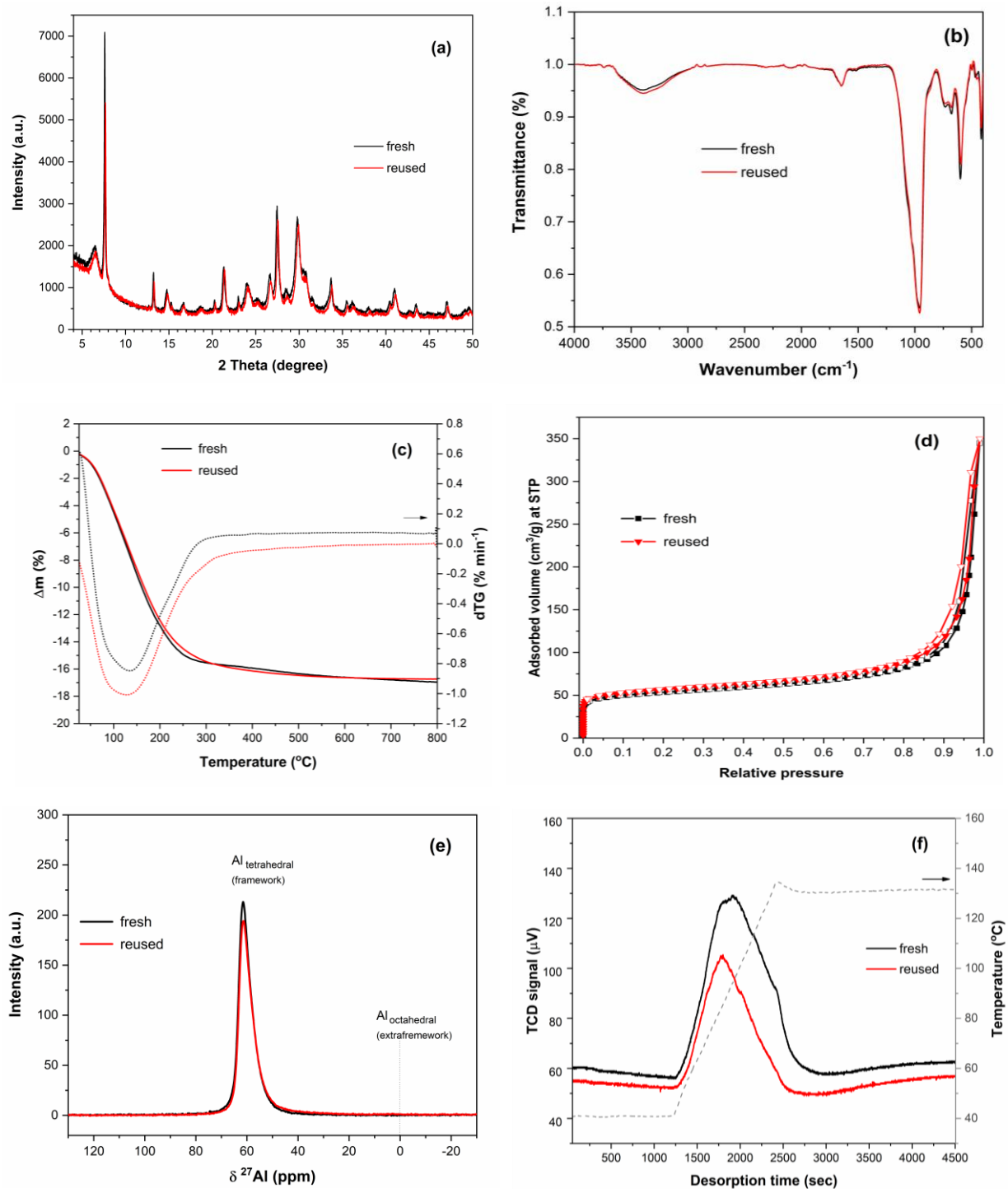

Fig. 9 Comparison between the fresh nano-sized CsBPH_AP and the reused sample after the fourth run by (a) XRD patterns, (b) FTIR spectra, (c) TG profiles, (d) N_2 sorption isotherms, (e) ^{27}Al MAS NMR spectra, and (f) CO_2-TPD profiles.

4. CONCLUSIONS

Physicochemical properties of as-prepared nano-sized and micron-sized BPH from hydrothermal methods (nano-sized CsBPH_AP and micron-sized KBPH_AP) and ion-exchanged samples (nano-sized K-CsBPH_IE and micron-sized Cs-KBPH_IE) are compared. The nano-sized samples have smaller particle sizes and thickness (192±15 nm vs. 541±40 nm), higher Si/Al ratios (1.33 vs. 1.00), and lower basicity. The ion-exchange process of nano-sized CsBPH_AP with potassium does not change the cesium content in the nano-sized sample but decreases the sodium content and lowers the basicity. On the other hand, the ion-exchange process of micron-sized KBPH_AP with cesium lowers the K content and increases the basicity.

The catalytic performances of the BPH zeolites for the transesterification of Gly with DMC are ranked in the following order: nano-sized CsBPH_AP > nano-sized K-CsBPH_IE > micron-sized Cs-KBPH_AP > micron-sized KBPH_AP. The better performance of the nano-sized zeolites, despite the lower basicity, is due to the influence of morphology and particle size. Smaller particles, specifically a reduction in the length along the *c*-axis, allows for better diffusion of the reactants and products through the zeolite pore network. Where catalytsts with similar morphologies and particle sizes are compared, the zeolite with the higher basicity displays better performance.

The optimum reaction condition of the best catalyst, nano-sized CsBPH_AP is 120 ºC for 3 h with a catalyst loading of 6 wt % and Gly:DMC molar ratio of 1:5. After four runs the nano-sized sample exhibits good stability in terms of structure and morphology, but a slight decrease in basicity. Overall, this work demonstrates that nano-sized CsBPH_AP is a promising catalyst

for the transesterification of Gly to produce GC and may find further application in other base-catalysed reactions.

Graphical abstract

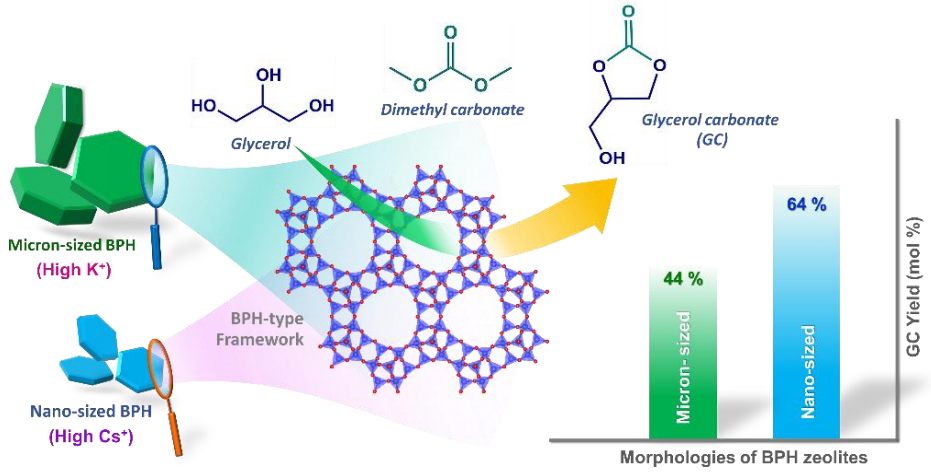

AUTHOR INFORMATION

Corresponding Authors

Jatuporn Wittayakun – School of Chemistry, Institute of Science, Suranaree University of Technology, Nakhon Ratchasima 30000, Thailand, orcid.org/0000-0002-4426-2825; E-mail: jatuporn@g.sut.ac.th

Edwin B. Clatworthy, Normandie Université, ENSICAEN, UNICAEN, CNRS, Laboratoire Catalyse et Spectrochimie (LCS), 14050 Caen, France, orcid.org/0000-0002-7204-2213; E-mail: edwin.clatworthy@ensicaen.fr

Authors

Siriporn Kosawatthanakun, School of Chemistry, Institute of Science, Suranaree University of Technology, Nakhon Ratchasima 30000, Thailand, orcid.org/0000-0002-6637-6049; E-mail: kosa.siriporn@gmail.com

Sajjad Ghojavand, Normandie Université, ENSICAEN, UNICAEN, CNRS, Laboratoire Catalyse et Spectrochimie (LCS), 14050 Caen, France, orcid.org/0000-0003-4136-2406; E-mail: sajjad.ghojavand@ensicaen.fr

Narongrit Sosa, Nuclear Technology Research and Development Center, Thailand Institute of Nuclear Technology (Public Organization), Nakhon Nayok 26120, Thailand, orcid.org/0000-0002-7745-329X; E-mail: narongrit.sci@gmail.com

Svetlana Mintova, Normandie Université, ENSICAEN, UNICAEN, CNRS, Laboratoire Catalyse et Spectrochimie (LCS), 14050 Caen, France, orcid.org/0000-0002-0738-5244; E-mail: svetlana.mintova@ensicaen.fr

Notes

The authors declare no competing financial interest.

ACKNOWLEDGMENTS

Kosawatthanakun, S. is supported by the Royal Golden Jubilee Ph.D. program (Grant No. PHD/0142/2557) from the Thailand Research Fund (TRF) and The French Embassy in Thailand with contribution to the RGJ-Ph.D. program. The financial support from the Centre of zeolites and nanoporous materials, Region Normandie, CNRS (CLEAR) is acknowledged.

REFERENCES

1. G. M. Mathew, D. Raina, V. Narisetty, V. Kumar, S. Saran, A. Pugazhendi, R. Sindhu, A. Pandey and P. Binod, Recent advances in biodiesel production: Challenges and solutions, *Sci. Total Environ.*, 2021, **794**, 148751.
2. G. Dodekatos, S. Schünemann and H. Tüysüz, Recent Advances in Thermo-, Photo-, and Electrocatalytic Glycerol Oxidation, *ACS Catal.*, 2018, **8**, 6301-6333.
3. B. A. Qureshi, X. Lan, M. T. Arslan and T. Wang, Highly active and selective nano H-ZSM-5 catalyst with short channels along b-axis for glycerol dehydration to acrolein, *Ind. Eng. Chem. Res.*, 2019, **58**, 12611-12622.
4. Q. M. She, W. J. Huang, A. Talebian-Kiakalaieh, H. Yang and C. H. Zhou, Layered double hydroxide uniformly coated on mesoporous silica with tunable morphorlogies for catalytic transesterification of glycerol with dimethyl carbonate, *Appl. Clay Sci.*, 2021, **210**, 106135.
5. H. W. Tan, A. R. Abdul Aziz and M. K. Aroua, Glycerol production and its applications as a raw material: A review, *Renew. Sustain. Energy Rev.*, 2013, **27**, 118-127.
6. W. A. Khanday, P. U. Okoye and B. H. Hameed, Biodiesel byproduct glycerol upgrading to glycerol carbonate over lithium–oil palm ash zeolite, *Energy Convers. Manag.*, 2017, **151**, 472-480.
7. Y. T. Algoufi and B. H. Hameed, Synthesis of glycerol carbonate by transesterification of glycerol with dimethyl carbonate over K-zeolite derived from coal fly ash, *Fuel Process. Technol.*, 2014, **126**, 5-11.
8. S. Pan, L. Zheng, R. Nie, S. Xia, P. Chen and Z. Hou, Transesterification of glycerol with dimethyl carbonate to glycerol carbonate over Na–based zeolites, *Chinese J. Catal.*, 2012, **33**, 1772-1777.

9. S. Wang, P. Hao, S. Li, A. Zhang, Y. Guan and L. Zhang, Synthesis of glycerol carbonate from glycerol and dimethyl carbonate catalyzed by calcined silicates, *Appl. Catal. A: Gen.*, 2017, **542**, 174-181.

10. M. Xiang and D. Wu, Transition metal-promoted hierarchical ETS-10 solid base for glycerol transesterification, *RSC Adv.*, 2018, **8**, 33473-33486.

11. P. Liu, M. Derchi and E. J. M. Hensen, Promotional effect of transition metal doping on the basicity and activity of calcined hydrotalcite catalysts for glycerol carbonate synthesis, *Appl. Catal. B: Environ.*, 2014, **144**, 135-143.

12. L. Wang, J. Zhang, S. Yang, Q. Sun, L. Zhu, Q. Wu, H. Zhang, X. Meng and F.-S. Xiao, Sulfonated hollow sphere carbon as an efficient catalyst for acetalisation of glycerol, *J. Mater. Chem. A* . 2013, **1**, 9422-9426.

13. H. Zhang, Z. Hu, L. Huang, H. Zhang, K. Song, L. Wang, Z. Shi, J. Ma, Y. Zhuang, W. Shen, Y. Zhang, H. Xu and Y. Tang, Dehydration of Glycerol to Acrolein over Hierarchical ZSM-5 Zeolites: Effects of Mesoporosity and Acidity, *ACS Catal.*, 2015, **5**, 2548-2558.

14. M. Moliner, C. Martinez and A. Corma, Multipore zeolites: synthesis and catalytic applications, *Angew. Chem. Int. Ed.*, 2015, **54**, 3560-3579.

15. K. J. Andries, H. J. Bosmans and P. J. Grobet, The crystal structure of zeolite Linde Q: A proposal based on powder X-ray diffraction and 27Al and 29Si MAS n.m.r. spectroscopy, *Zeolites*, 1991, **11**, 124-131.

16. B. D.W. and A. N.A., *US Pat.*, 2 991 151, 1961.

17. C. S. Blackwell, R. W. Broach, M. G. Gatter, J. S. Holmgren, D. Y. Jan, G. J. Lewis, B. J. Mezza, T. M. Mezza, M. A. Miller, J. G. Moscoso, R. L. Patton, L. M. Rohde, M. W.

Schoonover, W. Sinkler, B. A. Wilson and S. T. Wilson, Open-framework materials synthesized in the TMA+/TEA+ mixed-template system: the new low Si/Al ratio zeolites UZM-4 and UZM-5, *Angew Chem Int Ed Engl*, 2003, **42**, 1737-1740.

18. G. J. Lewis, J. G. Moscoso, M. A. Miller and B. A. Wilson, *US Pat.*, 6 419 895 B1, 2002.
19. B. A. Wilson, G. J. Lewis, D.-Y. Jan, S. T. Wilson and R. L. Patton, *US Pat.*, 6 776 975 B2, 2004.
20. E. B. Clatworthy, M. Debost, N. Barrier, S. Gascoin, P. Boullay, A. Vicente, J.-P. Gilson, J.-P. Dath, N. Nesterenko and S. Mintova, Room-Temperature Synthesis of BPH Zeolite Nanosheets Free of Organic Template with Enhanced Stability for Gas Separations, *ACS Appl. Nano Mater.*, 2020, **4**, 24-28.
21. W. Xie and H. Li, Alumina-supported potassium iodide as a heterogeneous catalyst for biodiesel production from soybean oil, *J. Mol. Catal. A Chem.*, 2006, **255**, 1-9.
22. S. Arora, V. Gosu and V. Subbaramaiah, One-pot synthesis of glycerol carbonate from glycerol using three-dimensional mesoporous silicates of K/TUD-1 under environmentally benign conditions, *Mol. Catal.*, 2020, **496**.
23. S.-T. Yang, J. Kim and W.-S. Ahn, CO_2 adsorption over ion-exchanged zeolite beta with alkali and alkaline earth metal ions, *Micropor. Mesopor. Mat.*, 2010, **135**, 90-94.
24. K. S. Walton, M. B. Abney and M. Douglas LeVan, CO_2 adsorption in Y and X zeolites modified by alkali metal cation exchange, *Micropor. Mesopor. Mat.*, 2006, **91**, 78-84.
25. Y.-K. Ma, S. Rigolet, L. Michelin, J.-L. Paillaud, S. Mintova, F. Khoerunnisa, T. J. Daou and E.-P. Ng, Facile and fast determination of Si/Al ratio of zeolites using FTIR spectroscopy technique, *Micropor. Mesopor. Mat.*, 2021, **311**.

26. K. J. Andries, B. D. Wit, P. J. Grobet and H. J. Bosmans, The synthesis and properties of synthetic zeolite Linde Q, *Zeolites*, 1991, **11**, 116-123.

27. W. Mozgawa, M. Król and K. Barczyk, FT-IR studies of zeolites from different structural groups, *Chemik*, 2011, **65**, 667-674.

28. A. Al-Ani, R. J. Darton, S. Sneddon and V. Zholobenko, Nanostructured zeolites: the introduction of intracrystalline mesoporosity in basic faujasite-type catalysts, *ACS Appl. Nano Mater.*, 2018, **1**, 310-318.

29. G. Busca, Acidity and basicity of zeolites: A fundamental approach, *Micropor. Mesopor. Mat.*, 2017, **254**, 3-16.

30. A.-P. Beltrao-Nunes, R. Sennour, V.-A. Arus, S. Anoma, M. Pires, N. Bouazizi, R. Roy and A. Azzouz, CO_2 capture by coal ash-derived zeolites- roles of the intrinsic basicity and hydrophilic character, *J. Alloys Compd.*, 2019, **778**, 866-877.

31. G. D. Pirngruber, P. Raybaud, Y. Belmabkhout, J. Cejka and A. Zukal, The role of the extra-framework cations in the adsorption of CO_2 on faujasite Y, *Phys. Chem. Chem. Phys.*, 2010, **12**, 13534-13546.

32. W. J. Mortier, Zeolite electronegativity related to physicochemical properties, *J. Catal.*, 1978, **55**, 138-145.

33. W. K. Teng, R. Yusoff, M. K. Aroua and G. C. Ngoh, Process optimization and kinetics of microwave assisted transesterification of crude glycerol for the production of glycerol carbonate, *Sustain. Energy Fuels*, 2021, **5**, 274-282.

34. S. Mintova, J. Grand and V. Valtchev, Nanosized zeolites: Quo Vadis?, *C R Chem.*, 2016, **19**, 183-191.

35. B. Das and K. Mohanty, A green and facile production of catalysts from waste red mud for the one-pot synthesis of glycerol carbonate from glycerol, *J. Environ. Chem. Eng.*, 2019, **7**, 102888.